Ji, C., Cabas, A., Cotton, F., Pilz, M., Bindi, D. (2020): Within-Station Variability in Kappa: Evidence of Directionality Effects. - Bulletin of the Seismological Society of America, 110, 3, 1247-1259.

https://doi.org/10.1785/0120190253

Within-Station Variability in Kappa: Evidence of Directionality Effects

Chunyang Ji*[1], Ashly Cabas[1], Fabrice Cotton[2,3], Marco Pilz[2], and Dino Bindi[2]

ABSTRACT

One of the most commonly used parameters to describe seismic attenuation is the high-frequency spectral decay parameter Kappa (κ_r), yet the physics behind it remain little understood. A better understanding of potential factors that lead to large scatter in estimated values of κ_r constitutes a critical need for ground-motion modeling and seismic hazard assessment at large. Most research efforts to date have focused on studying the site-to-site and model-to-model variability of κ, but the uncertainties in individual κ_r estimations associated with different events at a selected site (which we refer to as the within-station variability of κ_r) remain uncharacterized. As a direct corollary, obtaining robust estimates of the site-specific component κ_0, and their corresponding interpretation become a challenge. To understand the sources of the variability observed in κ_r (and κ_0) at a single site, we select 10 Japanese Kiban–Kyoshin network (KiK-net) downhole arrays and investigate the systematic contributions from ground-motion directionality. We observe that κ_r estimated from a single horizontal component is orientation dependent. In addition, the influence of ground-motion directionality is a function of local site conditions. We propose an orientation-independent κ_r-value, which is not affected either by ground-motion directionality or by the events' azimuths. In addition, we find that focal depth of events used in κ_r calculations affects the estimation of the regional attenuation component κ_R, which, in turn, influences the within-station variability in the κ_0 model.

KEY POINTS

- We study the within-station variability of kappa and the effects of record directionality and seismicity.
- The within-station variability of site-specific kappa is affected by ground-motion orientation and focal depth.
- Using the appropriate dataset and suggested orientation-independent kappa can help control kappa uncertainty.

Supplemental Material

INTRODUCTION

The characterization of attenuation at various scales (from regional to local) constitutes a critical component in the prediction of ground motions, site response analysis, and seismic hazard assessments. Thus, understanding ground-motion characteristics at high frequencies has become a research focus in recent studies (e.g., Mayor et al., 2018; Parolai, 2018). The high-frequency decay parameter κ was proposed by Anderson and Hough (1984) to characterize linear decay of the shear waves (S wave) Fourier amplitude spectrum (FAS) in log–linear scale in the high-frequency range. In general, individual estimations of κ values, hereafter referred to as κ_r, are decomposed into a site-specific component κ_0, a generalized distance-dependency component $\tilde{\kappa}_R$, and a source component κ_s (Ktenidou et al., 2014).

The site-specific component κ_0 captures the attenuation taking place directly below the site of interest (Ktenidou et al., 2013), but further investigation is required to define the depth of the geologic profile that contributes toward the

1. Department of Civil, Construction, and Environmental Engineering, North Carolina State University, Raleigh, North Carolina, U.S.A.
2. GFZ German Research Centre for Geosciences, Potsdam, Germany
3. University of Potsdam, Institute for Earth Sciences, Potsdam, Germany

*Corresponding author: cji3@ncsu.edu

κ_0 resulting at the ground surface. Ground-motion models (GMMs) and their adjustments from host to target regions have used estimates of κ_0 to characterize the effects of high-frequency attenuation (e.g., Campbell, 2003; Van Houtte et al., 2011; Ktenidou et al., 2014). Moreover, knowledge of κ_0 benefits the identification of epistemic uncertainties to remove the ergodic assumption in site-specific probabilistic seismic hazard analysis (PSHA), which is crucial for the seismic design of critical facilities such as nuclear power plants (Rodriguez-Marek et al., 2014; Cabas and Rodriguez-Marek, 2017). Deciphering the physics behind empirical estimates of κ_0 requires understanding the site's contribution to the overall attenuation. Decoupling local and regional attenuation mechanisms will facilitate the development of physics-based ground-motion simulations and nonergodic ground-motion prediction equations.

Previous studies have investigated the correlation between κ_0 and other site parameters such as the time-averaged shearwave velocity of the top 30 m subsoil (V_{S30}) (e.g., Van Houtte et al., 2011, 2014; Ktenidou et al., 2015; Cabas et al., 2017), but large uncertainties in κ_r estimations (which also affect the computation of κ_0) impose difficulties to unveil the physical meaning of κ_0 (Perron et al., 2017). An understanding of the sources of variability affecting κ_r and κ_0 constitutes a crucial step toward robust and sustainable applications of κ_0 in earthquake engineering practice.

The variability of κ has been studied through different lenses in the last decade, from model-to-model variability (e.g., Ktenidou et al., 2014; Edwards et al., 2015; Perron et al., 2017), user-to-user variability (e.g., Douglas et al. 2010; Edwards et al., 2015), to site-to-site variability (e.g., Van Houtte et al. 2011, 2014; Cabas et al. 2017). Some have investigated the variability in κ_r and κ_0 estimates when utilizing a single methodology, but incorporating alternative assumptions throughout the implementation (e.g., Ktenidou et al., 2013). Other efforts have focused on understanding the correlation (or lack thereof) among different methods to obtain κ_0 (e.g., Ktenidou et al., 2014; Perron et al., 2017). Whereas the variability of κ_0 as a function of site conditions have been extensively studied for multiple regions including Japan, Greece, France, and the United States (e.g., Douglas et al., 2010; Laurendeau et al., 2013; Ktenidou et al., 2015; Cabas et al., 2017; Parolai, 2018).

The objective of this study is to characterize the within-station variability of κ_0. Ten stations from the Japanese database, KiK-net, are investigated. Their corresponding National Earthquake Hazards Reduction Program (NEHRP) site class classification varies from B (rock) to D (stiff soils). First, we introduce a framework to evaluate aleatory variability and epistemic uncertainty in κ_r and κ_0. Then, we focus on individual values of κ_r calculated following the traditional approach by Anderson and Hough (1984) at the 10 study sites, and investigate how ground-motion directionality affects the estimation of κ_r. Finally, we explore the influence of earthquake type and focal depth on the estimates of κ_R and κ_0. Within one selected station, we find that the values of κ_R and κ_0 are affected by repeatable contributions from the path, with these path effects being more significant for κ_R.

UNCERTAINTY AND VARIABILITY IN KAPPA

Empirical data from multiple seismic events and recording stations are used to construct GMMs that can describe the distribution of ground motion in terms of a median and a logarithmic standard deviation σ (Al Atik et al., 2010). The aleatory variability in the ground motion, represented by σ has proven to exert a strong influence on hazard estimates, especially at low annual exceedance frequencies (Bommer and Abrahamson, 2006; Al Atik et al., 2010; Rodriguez-Marek et al., 2014). Defensible reductions in σ are desirable not only because of their ultimate effect on PSHA, but also because they result from a clear separation of aleatory

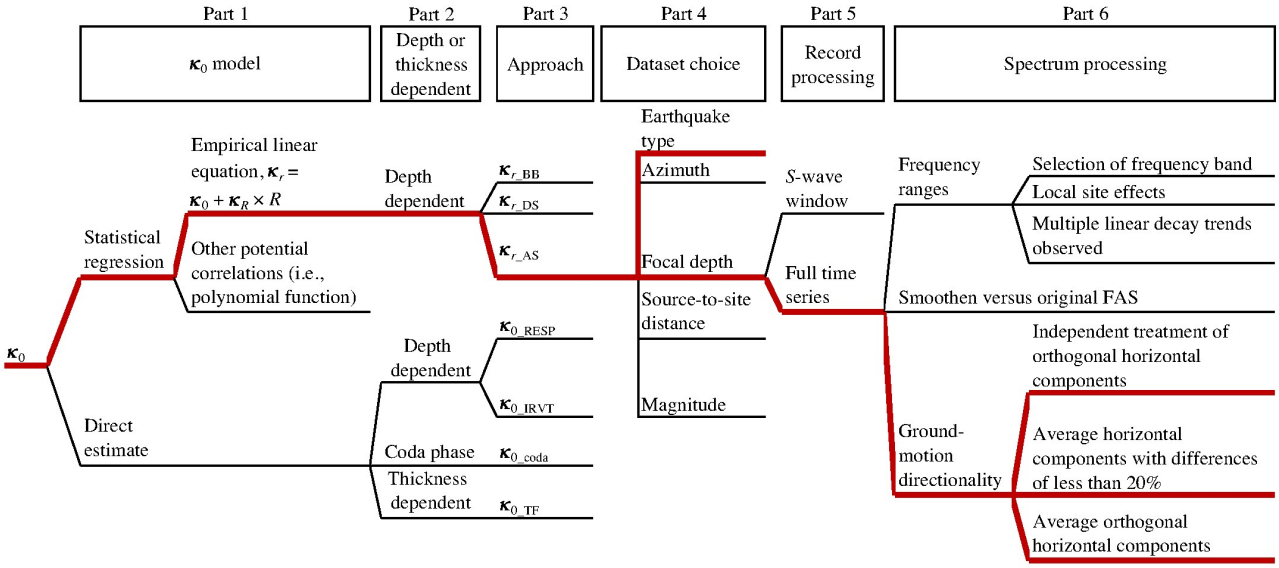

Figure 1. *Logic tree for the estimation of κ0 values. The highlighted branches are explored in this work. FAS, Fourier amplitude spectrum.*

variability (which is theoretically irreducible) and epistemic uncertainty (which can be reduced with the collection of new data; Rodriguez-Marek et al., 2014). In pursuit of defensible reductions in σ, repeatable source, path, and/or site contributions can be identified at a single site and invoke the nonergodic assumption. The ergodic assumption implies that the temporal distribution of ground motions at a given site is equivalent to the spatial distribution of ground motions across many sites (given the same causal parameters; Kuehn et al., 2019).

In this study, we focus on identifying repeatable site and path contributions to the observed variability in κ_r, κ_R, and κ_0. Drawing parallels to the residual analysis process in ground-motion modeling, this work aims to provide a characterization of the within-station variability in κ_r and κ_0 estimates, which can further support the development of the site-term parameterization in nonergodic GMMs. Baltay et al. (2017) provided evidence of a correlation between κ_0 values and the average site residual, using small-magnitude ground-motion data recorded at 10 stations from the ANZA network. Estimates of κ_0 could inform predictions of station-specific site residuals in partially nonergodic GMMs "to improve our physical understanding of the site term at specific stations" (Baltay et al., 2017, p. 1767).We select a subset of recordings at selected stations from the KiK-net database to identify and quantify systematic, repeatable contributions to κ_r, κ_R, and κ_0 estimates; hereafter referred to as within-station variability in κ.

Approaches to estimate κ_0 can be classified into two types, namely direct estimates and empirical estimates from statistical regressions. Factors that introduce variability in κ_0 estimates for each type are grouped into six categories with considerations of model selections, database choices, and record processing protocols as shown in Figure 1. The latter provides a framework to investigate epistemic uncertainties in κ_0 estimates for the linear elastic regime only. Further research is required should soil nonlinearity be triggered. The description of each category depicted in Figure 1 is presented subsequently.

Part 1 κ_0 model: The commonly used statistical regression approach is based on a linear distance-dependent model, in which κ_0 represents the site-specific component, whereas κ_R refers to the regional attenuation. Values of κ_0 and κ_R are obtained via empirical linear regression of κ_r following the Anderson and Hough (1984) method. Alternatively, direct estimates of κ_0 can

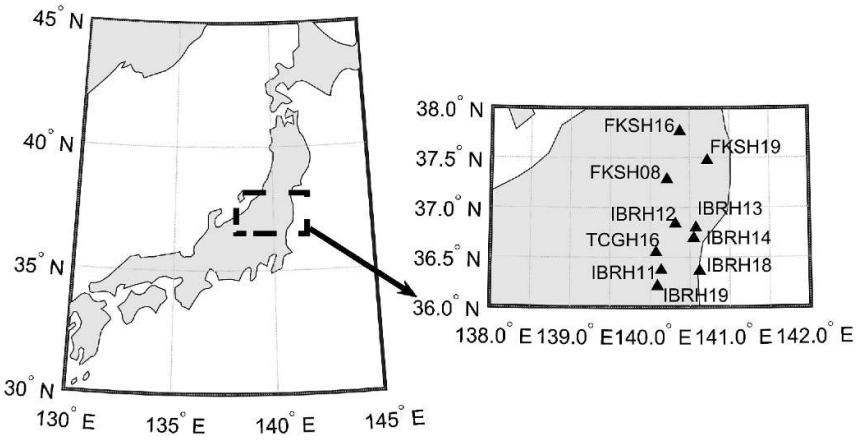

Figure 2. *Locations of each selected Japanese station in this study.*

be obtained from the site properties (e.g., measurements of κ_0 in the high-frequency decay of a transfer function; Drouet et al., 2010) without the definition of the κ_0-linear regression model. The choice of a linear regression, as opposed to other possible functional forms, has been mostly based on the simplicity of the model and observed fit to the empirical data (Ktenidou et al., 2013).

Part 2 depth dependency: The measured κ_0 values can be depth dependent or thickness dependent, based on the approach selected for the respective calculations. Values of κ_0 provide an estimate of attenuation directly below the depth at which the ground motions are recorded. Different κ_0 values are typically obtained at different depths within a site profile (e.g., Ktenidou et al., 2015). Values of site-specific κ_0 have also been proposed to represent the contribution of a specific soil column with a given thickness (e.g., Campbell, 2009).

Part 3 approach choice: Previous studies show that various kappa calculation approaches will result in different individual κ_r values (for the same ground motion), and ultimately different κ_0 estimates (e.g., Ktenidou et al., 2014). Understanding the suitability of each method in consideration of the available records and site conditions is relevant to reduce uncertainties in kappa estimations. In Figure 1, $\kappa_{r_{BB}}$, $\kappa_{r_{DS}}$, and $\kappa_{r_{AS}}$ refer to individual values of kappa from the broadband method (Ktenidou et al., 2016), the displacement method (Biasi and Smith, 2001), and the acceleration spectrum method (Anderson and Hough, 1984), respectively. Direct measurement approaches, also shown in Figure 1, include estimations of κ_0 from the response spectrum ($\kappa_{0_{\mathrm{RESP}}}$; Silva and Darragh, 1995), utilizing inverse random vibration theory ($\kappa_{0_{\mathrm{IVRT}}}$; Al Atik et al., 2014), and from the site's transfer function ($\kappa_{0_{\mathrm{TF}}}$; Drouet et al., 2010).

Part 4 dataset choice: Choosing an appropriate dataset can reduce the within-station variability in κ_0 by constraining the uncertainties associated with individual κ_r values. In general, only magnitude, source-to-site distance, and type of seismicity are used to select appropriate ground motions for kappa calculations. However, we hypothesize that considering the events' azimuth and focal depths can provide insights on other sources of within-station variability.

Part 5 record processing: The variability associated with record processing refers to differences stemming from the usage of the S-wave window or the whole time series to calculate κ_r values. Anderson and Hough (1984) originally introduced the calculation of $\kappa_{r_{AS}}$ as the linear decay of the S-wave FAS in the high-frequency range. However, varying selections of the S-wave window can introduce additional scatter in κ_r for the same event (Douglas et al., 2010; Cabas et al., 2017; Xu et al., 2019). This additional variability may be caused by the assumed duration of the selected S-wave window, the explicit consideration of the direct S wave only, or the potential mix of the direct S-wave window with coda or surface waves. Values of $\kappa_{r_{AS}}$ estimated from the S-wave window could be significantly biased by scattering effects, except when intrinsic attenuation is dominant (Parolai et al.,

TABLE 1
Selected Station Information

Station Name	Station Latitude (°)	Station Longitude (°)	V_{S30} (m/s)*	Hole Depth (m)†	H_{800} (m)#	Borehole Sensor Azimuth (°)	NEHRP Site Class§
FKSH08	37,28	140,22	562,50	105	8	-3	C
FKSH16	37,76	140,38	531,61	300	180	1	C
FKSH19	37,47	140,73	338,06	100	20	-4	D
IBRH11	36,37	140,14	242,49	103	30	0	D
IBRH12	36,83	140,32	485,71	200	20	-3	C
IBRH13	36,79	140,58	335,37	100	34	2	D
IBRH14	36,69	140,55	829,12	100	10	-1	B
IBRH18	36,36	140,62	558,56	504	30	0	C
IBRH19	36,21	140,09	692,31	210	2	-1	C
TCGH16	36,54	140,08	213,20	112	NaN	-2	D

2015; Pilz and Fäh, 2017; Parolai, 2018; Pilz et al., 2019).

Part 6 spectrum processing: The estimation of $\kappa_{r_{AS}}$ is significantly sensitive to the selection of frequency ranges, including: (1) the length of the frequency band, (2) local site conditions such as site-amplification peaks (Parolai and Bindi, 2004), and (3) the presence of multiple linear decay trends in the high-frequency range of the FAS. Using smoothen FAS instead of the original FAS also introduces differences for κ_r estimates. In addition, there is a variability resulting from different approaches to treat recorded horizontal components. For instance, (1) treating orthogonal horizontal components independently (Dimitriu et al., 2001), (2) averaging $\kappa_{r_{AS}}$ values estimated from as-recorded horizontal components if differences in these $\kappa_{r_{AS}}$ values are less than 20% (Ktenidou et al., 2013), and (3) averaging $\kappa_{r_{AS}}$ values estimated from as-recorded horizontal components without consideration of the corresponding differences in individual $\kappa_{r_{AS}}$.

We would like to emphasize that the ultimate influence of the aforementioned sources of variability is usually station dependent, although the logic tree and framework described in Figure 1 can be implemented at any site. Thus, the significance of each branch is unique for a given site, which results in a better characterization of the within-station variability at the site. In this article, we only focus on the branches highlighted in Figure 1. The Anderson and Hough (1984) method is used to investigate systematic contributions to the variability in κ_r (hereafter referred to as $\kappa_{r_{AS}}$) and κ_0. We investigate the within-station variability caused by (1) the dataset choice (part 4) based on earthquake types and focal depths and (2) spectrum processing (part 6) by understanding the contributions of ground-motion directionality.

DATABASE DESCRIPTION AND STUDY SITES

We use the Japanese Kiban–Kyoshin network (KiK-net) database (see Data and Resources), which is a strong-motion seismograph network uniformly deployed at more than 600 locations in Japan and able to provide high-quality data at various site classes. KiK-net has a pair of seismographs at each station, one located on the ground surface and the other one in a borehole together with high-sensitivity (Hi-net) seismographs. The depth of each borehole sensor is typically between 100 and 200 m. Instrumental sampling frequencies are 100 or 200 Hz. Wave velocity profiles (for both *P* and *S* wave) at each station are measured by downhole *PS* logging, and the corresponding files are available on the KiK-net website (see Data and Resources). The orientations of orthogonal ground surface sensors are north–south and east–west. However, difficulties during installation and regular maintenance at some stations may have changed the orientations of borehole sensors

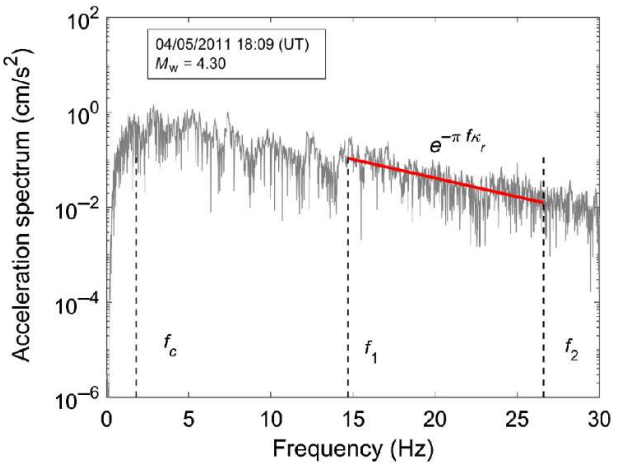

Figure 3. *Selection of f_1 and f_2 on the FAS corresponding to a surface record at station IBRH20. f_c refers to the corner frequency as estimated by the Brune (1970) model with stress drop of 3.0 MPa for active crustal events.*

(Aoi et al., 2004; Aoi et al., 2011). The azimuths of borehole sensors at each KiK-net station are available on the Hi-net website (see Data and Resources). The entire dataset and flatfile used in this article is built and compiled with an automated protocol by Dawood et al. (2016). The seismic moment magnitude M_w, focal depth, epicenter location, and focal mechanism information are obtained from the Natural Research Institute for Earth Science and Disaster Prevention (NIED) moment tensor solution available at the broadband seismography network (F-net) catalog.

In this article, recorded horizontal components at the ground surface and at depth are used. The criteria for selection of ground motions and stations include: (1) epicentral distances less than 150 km, (2) M_w larger than 4.0, (3) peak ground acceleration (PGA) values at the surface less than 0.01g (to avoid effects of soil nonlinearity), (4) at least 50 available records complying with requirements (1–3) per study site, and (5) the signal-to-noise ratio larger 3.0 over the frequency ranges for $\kappa_{r_{AS}}$ estimation. Moreover, the ability of shear-wave velocity profiles measured by downhole logging at KiK-net stations to describe actual site conditions has been questioned in the past (Wu et al., 2017). 2D and 3D wave propagation could be significant at some KiK-net stations because of the edge-generated surface waves, topographic effects, and focusing effects. However, the potential for site scattering effects can be reduced as we considered KiK-net sites with reliable shear-wave velocity (V_S) profiles that meet the 1D wave propagation assumptions based on the results from Pilz and Cotton (2019). Thus, 10 stations corresponding to various site classes (NEHRP site class from B to D) are selected in this study. Key characteristics pertaining these study sites are provided in Figure 2 and Table 1.

METHODS

Estimation of κ_r and κ_0

We use the acceleration spectrum approach (Anderson and Hough, 1984) to estimate $\kappa_{r_{AS}}$. The slope of the linear decay $-\pi\kappa_{r_{AS}}$ of the acceleration FAS in the high-frequency range using log–linear coordinates is calculated for each horizontal component of the selected records. A weighted robust least-squares linear regression with bi-square function is applied over a manually selected high-frequency range ($[f_1, f_2]$) to fit the linear decay trend (see Fig. 3 as an example). The minimum difference between f_1 and f_2 is 8 Hz. Following the recommendations of Ktenidou et al. (2013), f_1 is larger than the corresponding earthquake source-corner frequency (f_c), computed by equation (1) (Brune, 1970, 1971):

$$f_c = 4.9 \times 10^4 \beta \left(\frac{\Delta\sigma}{M_0}\right)^{\frac{1}{3}}, \qquad (1)$$

in which f is in hertz, β is the shear-wave velocity near the source with units of kilometers per second, $\Delta\sigma$ is the stress drop in MPa, and M_0 is the seismic moment in newton·meter. In this article, β is assumed to be 3.6 km/s (Pei et al., 2009). The value of $\Delta\sigma$ is assumed to be 3MPa for crustal earthquakes and 5.5 MPa for subduction zone events (Nakano et al., 2015). Moreover, because the instrument's response is

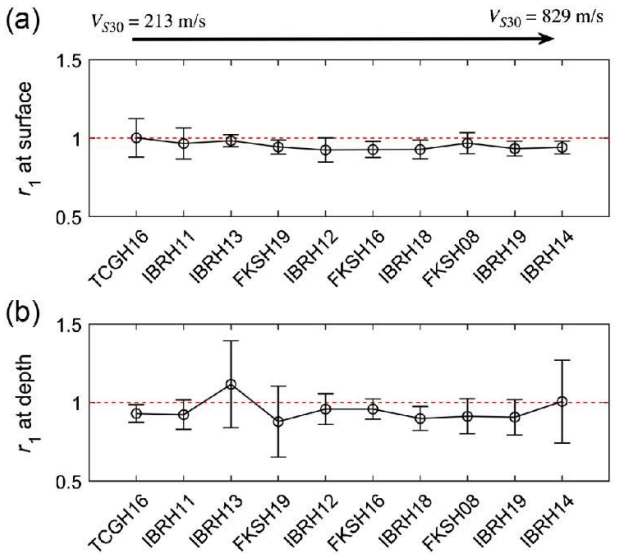

Figure 4. *Comparison between $\kappa_{r_{AS}}$ (from the whole FAS) and $\kappa_{r_{AS}SW}$ (from the S-wave window FAS) corresponding to our 10 study sites at (a) ground surface and (b) borehole. r_1 is the ratio computed by $\kappa_{r_{AS}} = \kappa_{r_{AS}SW}$. The dashed line represents a ratio of 1.0. The circles depict the mean r1 of all observed records, and the error bars indicate the _ standard derivation of all observed ratios at each site of interest.*

approximately flat below 30 Hz (which is close to the response of a three-pole Butterworth filter with a cutoff frequency of 30 Hz), we restrict f_2 to be less than 30 Hz (Aoi et al., 2004; Fujiwara et al., 2004; Oth et al., 2011; Laurendeau et al., 2013; Cabas et al., 2017).

The S-wave window is often used to estimate $\kappa_{r_{AS}}$. Previous studies have picked the direct S wave manually assuming a minimum duration of 5 s for small, nearby events and 20 s for large, far events (Ktenidou et al., 2013). Whereas others have included the coda wave within the selected S-wave window for records for which the coda wave cannot be separated clearly (Anderson and Hough, 1984). Differences in $\kappa_{r_{AS}}$ (computed by the acceleration spectrum approach using the whole time series) and $\kappa_{r_{AS}SW}$ (computed by the acceleration spectrum approach using manually selected S-wave windows, following Anderson and Hough, 1984) are compared for records from shallow crustal earthquakes used in this study (see Fig. 4). The same frequency range f_1 and f_2 is applied to each record to avoid bias from frequency range selections. The ratio $r_1 = \kappa_{r_{AS}}/\kappa_{r_{AS}SW}$ is computed at each study site to represent the differences between $\kappa_{r_{AS}}$ and $\kappa_{r_{AS}SW}$ in Figure 4. Values of $\kappa_{r_{AS}SW}$ are generally larger than $\kappa_{r_{AS}}$ at the study sites (i.e., r_1 is generally less than 1.0). Scattering effects can help explain observed lower $\kappa_{r_{AS}}$ values from the whole time series. When intrinsic attenuation is strong at a given site, higher frequencies can be removed more efficiently, resulting in a steep slope in the S-wave FAS (Parolai et al., 2015). The full time series is composed of the direct S waves, but also scattered waves from the redistribution of the seismic waves' energy. The latter can modify the slope in the FAS at high frequencies producing a biased $\kappa_{r_{AS}}$, which generally is lower. Moreover, the S-wave window dominates the spectrum at surface, and the down-going waves could more affect the borehole time series. Thus, more variations between $\kappa_{r_{AS}}$ and $\kappa_{r_{AS}SW}$ at depth are observed. Because the differences between $\kappa_{r_{AS}SW}$ and $\kappa_{r_{AS}}$ are less than 20% for most of the selected ground motions used in this study, we choose the full time series to estimate $\kappa_{r_{AS}}$ values. Further guidance in the selection of the S-wave window for kappa calculations can provide meaningful insights to reduce the between-station variability in kappa.

We choose the linear κ_0 model introduced by Anderson (1991) and follow the nomenclature proposed by Ktenidou et al. (2013) to estimate the site component κ_0:

$$\kappa_{r_{AS}} = \kappa_0 + \kappa_R \times R_{epic}, \qquad (2)$$

in which the $\kappa_{r_{AS}}$ and κ_0 are expressed in units of time (s), κ_R in units of kilometers per second, and R_{epic} is the epicentral distance in kilometers. This κ_0 model assumes a unique source-to-site path for each record, and a homogeneous, frequency-independent, seismic quality factor Q (Knopoff, 1964). Thus, we only select events with epicentral distances less than 150 km to

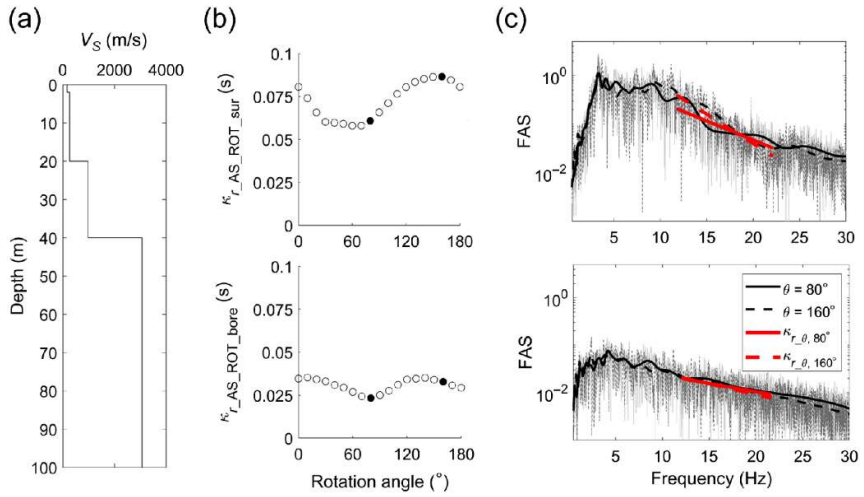

Figure 5. *Example of $\kappa_{r_{AS}\mathrm{ROT}}$ variations. (a) Shear-wave velocity profile at FKSH19, (b) comparison between $\kappa_{r_{AS}\mathrm{ROT}}$ and rotation angle at surface and borehole for one record, and (c) the FAS for rotated components with θ of 80° and 160°. The dark solid and dashed lines show the smoothen FAS to emphasize the differences between rotated FASs. The select ground motion was a shallow active crustal event recorded at FKSH19 (site class D) with seismic moment magnitude of 4.4, azimuth of 19°, and epicentral distance of 117 km (recorded on 26 July 2003 UTC).*

minimize the potential for multiple source-to-site ray paths per record. The assumption of a unique Q-value allows for the calculation of κ_R (following the linear model in equation 2), which describes regional attenuation. Japan has varying Q-values across the region, with lower Q-values in the central Japanese island and higher Q-values on the east coast (Pei et al., 2009; Nakano et al., 2015). The low Q- and high Q-value regions are separated by Japan's volcanic belt. Thus, we avoid using records that cross the volcanic belt during their propagation path from source-to-site based on the attenuation classification map provided by Nakano et al. (2015). The κ_0 model in equation (2) is also based on the assumption that the source contribution is negligible (Van Houtte et al., 2011; Ktenidou et al., 2014). For the selected KiK-net stations, the path component κ_R is constrained to be the same for both surface and borehole records because the regional attenuation contributions should be identical when analyzing individual stations (Ktenidou et al., 2013, 2015; Cabas et al., 2017). We use the maximum-likelihood method to model $\kappa_{r_{AS}}$ with the constrained κ_R based on equation (2).

Ground-motion directionality

A recorded ground motion at a specific site can vary depending on sensor orientation (Boore et al., 2006). This lack of uniformity of ground motions in all possible orientations is known as ground-motion directionality. Two as-recorded horizontal orthogonal components of each selected ground motion are rotated to study the influence of ground-motion directionality on the estimation of $\kappa_{r_{AS}}$. All records are rotated using the following equations (Boore et al., 2006; Boore, 2010):

$$a_{\mathrm{ROT}_1}(t;\theta) = a_1(t)\cos(\theta) + a_2(t)\sin(\theta), \quad (3)$$

$$a_{\mathrm{ROT}_2}(t;\theta) = a_1(t)\sin(\theta) + a_2(t)\cos(\theta), \quad (4)$$

in which $a_1(t)$ and $a_2(t)$ are the as-recorded acceleration time series, $a_{\mathrm{ROT}_1}(t;\theta)$ and $a_{\mathrm{ROT}_2}(t;\theta)$ are the rotated motions with the corresponding rotation angle θ. The $\kappa_{r_{AS}}$ values computed from the corresponding FAS of rotated motions are referred to as $\kappa_{r_{AS}\mathrm{ROT}}$. In this article, we use either equation (3) or (4) to rotate the as-recorded horizontal components from 0° to 180° (i.e., nonredundant angles) with increments of 10° to investigate the influence of ground-motion directionality on $\kappa_{r_{AS}}$.

Considering that the frequency range ($[f_1, f_2]$) to estimate $\kappa_{r_{AS}}$ is selected visually for each event, a large number of calculations is required for $\kappa_{r_{AS}\mathrm{ROT}}$ estimations. Thus, we propose a semiautomatic algorithm to compute $\kappa_{r_{AS}\mathrm{ROT}}$. First, we select the frequency range based on visual inspection of the as-recorded motion from a given event (at a given site). Then, a common frequency range is selected for

the pair of recorded horizontal components and applied to all the corresponding rotated motions from that same event at that station. The main advantage of the proposed procedure, beyond the optimization of the computational process, is that it avoids the introduction of additional uncertainties stemming from the frequency range selection. The performance of the proposed semiautomatic algorithm is evaluated by visually inspecting the rotated FAS plots and the corresponding frequency range.

The influence of ground-motion directionality on the attenuation contributed by the soil column, hereafter referred to as $\Delta\kappa(\theta)$, is also investigated. $\Delta\kappa(\theta)$ is calculated as follows, assuming the κ_R-value remains unchanged:

$$\begin{aligned}\Delta\kappa(\theta) &= \kappa_{r_{AS}\mathrm{ROT}_{sur}}(\theta) - \kappa_{r_{AS}\mathrm{ROT}_{bore}}(\theta)\\ &= \left(\kappa_{0_{\mathrm{ROT}}\mathrm{bore}}(\theta) + \kappa_R \times R_{epic}\right)\\ &- \left(\kappa_{0_{\mathrm{ROT}}\mathrm{sur}}(\theta) + \kappa_R \times R_{epic}\right)\\ &= \Delta\kappa_{0_{\mathrm{ROT}}}(\theta).\end{aligned} \quad (5)$$

It should be noted that errors in the azimuth of borehole sensors (i.e., sensors not oriented in the true north–south or east–west directions) could propagate through the estimation of $\Delta\kappa(\theta)$, which means that values of θ at the surface and at depth may not be consistent. The errors in the azimuth are observed at eight selected sites, and the maximum borehole sensor deflection is 4° (shown in Table 1). Thus, we correct the borehole record orientation with the azimuth of borehole sensors provided by Hi-net before the borehole horizontal component is rotated.

RESULTS AND DISCUSSION

Directionality effects on κ_r and κ_0 estimations

A variation of $\kappa_{r_{AS}\mathrm{ROT}}$ with rotation angle is observed for both surface and borehole records at all stations. Figure 5 presents an example of the relationship between $\kappa_{r_{AS}\mathrm{ROT}}$ and rotation angles at FKSH19. The corresponding FAS of the rotated components are also presented (i.e., with rotation angle of 80° and 160°) for comparison purposes, depicting changes of the decay in the high-frequency range. The standard derivations corresponding to $\kappa_{r_{AS}\mathrm{ROT}_{sur}}$ and $\kappa_{r_{AS}\mathrm{ROT}_{bore}}$ are 0. 0109 and 0.0041 s, respectively.

Figure 5 illustrates that the variation of $\kappa_{r_{AS}\mathrm{ROT}}$ at the surface is more significant than at depth, which is also observed for the majority of records across all stations. We then investigate the influence of the event azimuth on the maximum $\kappa_{r_{AS}\mathrm{ROT}}$ observed and its corresponding rotation angle. The rotation angle associated with the maximum $\kappa_{r_{AS}\mathrm{ROT}}$ is hereafter referred to as θ_{max}. A correlation between θ_{max} and the azimuth of each record at the surface and at depth is not found. The corresponding comparison between event azimuth and θ_{max} for each study site is presented in Figure S1, available in the supplemental material to this article, which supports our hypothesis that the maximum $\kappa_{r_{AS}\mathrm{ROT}}$ is affected by the local site condition rather than the event azimuth.

The mean of all $\kappa_{r_{AS}\mathrm{ROT}}$ for each record $\kappa_{r_{AS}\mathrm{mean}}$ and the average of $\kappa_{r_{AS}\mathrm{H1}}$ and $\kappa_{r_{AS}\mathrm{H2}}$ from the corresponding as-recorded horizontal components $\kappa_{r_{AS}\mathrm{ave}}$ are compared in Figure 6 by means of the ratio $r_2 = \kappa_{r_{AS}\mathrm{ave}}/\kappa_{r_{AS}\mathrm{mean}}$. Figure 6 demonstrates that the differences between $\kappa_{r_{AS}\mathrm{mean}}$ and $\kappa_{r_{AS}\mathrm{ave}}$ values at the ground surface are small; the maximum average of surface r_2 across the 10 study sites is 1.04 (at IBRH13; $V_{S30} = 335$ m/s) and the minimum average is 0.96 (at FKSH16; $V_{S30} = 532$ m/s).

However, at station IBRH14 ($V_{S30} = 829$ m/s), the differences of borehole $\kappa_{r_{AS}\mathrm{mean}}$ and $\kappa_{r_{AS}\mathrm{ave}}$ values are relatively large, with an average r_2 of 0.85 and a standard derivation of r_2 equal to 0.19. A closer inspection of the empirical transfer function (ETF) at this station reveals that $\kappa_{r_{AS}}$ estimates at IBRH14 could be affected by the site amplification in high frequencies, which can help explain observed differences

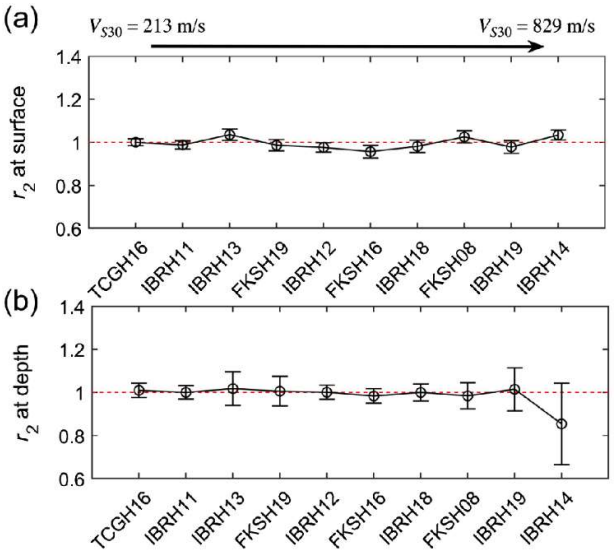

Figure 6. *Comparison between mean $\kappa_{r_{AS}}$ of rotated motions (i.e., $\kappa_{r_{AS}mean}$) and mean $\kappa_{r_{AS}}$ of two recorded horizontal component (i.e., $\kappa_{r_{AS}ave}$) at selected stations along with the corresponding standard derivation at (a) ground surface and (b) borehole. r_2 corresponds to the ratio $\kappa_{r_{AS}ave}/\kappa_{r_{AS}mean}$. The dashed line indicates an r_2 equal to 1.0, and the circles depict the mean r_2 across all records considered per station. The error bars indicate the standard deviation of all r_2 computed at each site of interest.*

between $\kappa_{r_{AS}\text{mean}}$ and $\kappa_{r_{AS}\text{ave}}$. The corresponding ETFs at IBRH13, FKSH08, FKSH16, and FKSH19 also show varying site-amplification in the high-frequency range. Differences between $\kappa_{r_{AS}\text{mean}}$ and $\kappa_{r_{AS}\text{ave}}$ for all study sites are also presented in Figure S2. In Figure S2, the different colors indicate the differences between $\kappa_{r_{AS}\text{H1}}$ and $\kappa_{r_{AS}\text{H2}}$, which show that the discrepancy between two horizontal components will not affect $\kappa_{r_{AS}\text{ROT}}$ and $\kappa_{r_{AS}\text{mean}}$. Considering the similarity observed between values of $\kappa_{r_{AS}\text{mean}}$ and $\kappa_{r_{AS}\text{ave}}$ for multiple ground motions and across study sites, an orientation-independent κ_r-value for one recorded event at a given station can be estimated from the average of $\kappa_{r_{AS}\text{H1}}$ and $\kappa_{r_{AS}\text{H2}}$ computed from as-recorded orthogonal horizontal components directly. In the following sections, we use $\kappa_{r_{AS}\text{ave}}$ (also denoted as $\kappa_{r_{AS}}$ for simplicity) as the representative value for each pair of orthogonal horizontal components.

The effects of ground-motion directionality on $\Delta\kappa(\theta)$ (equation 5) are also explored to investigate how the orientation of ground motion can affect the seismic attenuation taking place throughout the soil column. Figure 7 and Table 2 show the variations of $\Delta\kappa(\theta)$ at the sites of interest. First, we observe that the seismic attenuation contributed by the soil column is affected by ground-motion directionality. Second, there seems to be a systematic variation with directionality unique to each site, with the maximum $\Delta\kappa(\theta)$ generally corresponding to the same rotation angle across different ground motions at each station. Kotha et al. (2019) proved that the contribution of radiation pattern to the ground-shaking characteristics would be weak and random in the high-frequency range. Thus, we hypothesize that the influence of ground-motion directionality on the high-frequency parameter κ is station dependent and not affected by the earthquake source. Moreover, the maximum σ for $\Delta\kappa(\theta)$ is observed at FKSH16, which has a thick soil column (hole depth of 300 m and $H_{800} = 180$ m) and a $V_{S30} = 532$ m/s. The minimum σ-value is found at IBRH19 with H_{800} of 2 m, V_{S3} of 692 m/s, and hole depth of 210 m. However, a strong correlation between σ and H_{800} = or V_{S30} or hole depth is not evident across all study sites. Different site parameters (or a combination of existing ones) with considerations of shallow and deeper geologic structures are required to further detect potential correlations between site conditions and variability in $\Delta\kappa_0$ due to ground-motion directionality.

Finally, we compare the mean of all $\Delta\kappa(\theta)$ values with the difference between surface and borehole κ_0 values (hereafter referred to as $\Delta\kappa_0$) from empirical linear regressions conducted on as-recorded horizontal components (i.e., averaging as-recorded $\kappa_{r_{AS}}$ values for each pair) at each station (Fig. 8). Mean values of $\Delta\kappa(\theta)$ shown in Figure 8 are only slightly higher than the corresponding $\Delta\kappa_0$ values, which indicates that the mean of two as-recorded $\kappa_{r_{AS}}$ values can lead to an orientation-independent estimation of $\Delta\kappa_0$. Figure 8 also provides a

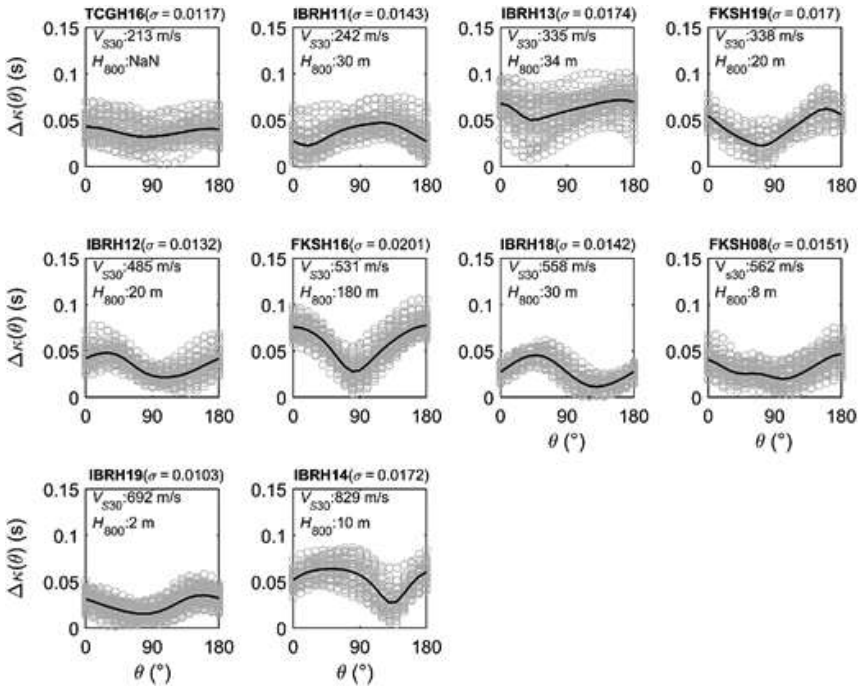

Figure 7. *Variability of* Δκ(θ) *at the stations of interest and the corresponding site information. The solid lines represent the mean of all* Δκ(θ) *across all records per rotation angle, whereas the gray circles depict* Δκ(θ) *obtained for each record and multiple rotation angles. H800 refers to depth to a horizon with velocity V_S of 800 m/s or more.*

comparison of the within-station and between-station variability of $\Delta\kappa(\theta)$. For most stations considered in this study (i.e., FKSH08, IBRH14, IBRH12, FKSH19, IBRH18, IBRH13, FKSH16, and IBRH11), the within-station variability in $\Delta\kappa(\theta)$ is comparable and sometimes more significant, which evidences the need for a more rigorous consideration of the within-station variability in κ_0 estimates. We note that the observed larger within-station variabilities in $\Delta\kappa(\theta)$ at IBRH13, IBRH14, FKSH08, FKSH16, and FKSH19 can be influenced by site-amplification effects at these sites in the high frequency. The latter can induce bias in the resulting κ values. The quantification of the within-station variability in κ will result in more reliable κ_0 estimates, which can inform empirical correlations with local site conditions.

Earthquake type and focal depth effects on κ_r, κ_R, and κ_0 estimations

In this section, we investigate the influence of earthquake type and focal depth on average $\kappa_{r_{AS}}$ from as-recorded components, regional attenuation, as captured by κ_R and κ_0 estimations. The algorithm proposed by Garcia et al. (2012) is used herein to classify earthquake types as: (1) shallow active crustal (ACRsh; if the hypocentral depth is less than 35 km), (2) deep active crustal (ACRde; if the hypocentral depth is larger than 35 km), (3) subduction zone intraslab (SZintra; with minimum focal depth of 15 km), and (4) subduction zone interface (SZinter) earthquakes (with minimum focal depth of 70 km).

Values of $\Delta\kappa_0$, $\kappa_{0_{sur}}$, $\kappa_{0_{bore}}$, and κ_R at the selected 10 stations are computed for different datasets categorized by earthquake type and shown in Figure 9. It should be noted that the limited number of ACRde events did not allow for the derivation of the corresponding κ_0 and κ_R for this particular dataset. A few negative values of κ_R and κ_0 values are obtained at some stations for some of the datasets, which could be caused by the lack of available events for each earthquake type at specific epicentral distance ranges. For example, ACRsh events recorded at IBRH11 only have epicentral distances in the range of 50–150 km. Hence, those cases were not included in Figure 9. The resulting κ_0 and κ_R values demonstrate that different seismicity types lead to varying estimates of the κ_R component (i.e., the slope of κ_0 model), which, in turn, affects the estimated site-specific κ_0 component (i.e., the intersect in the y axis at zero epicentral distance). Records from subduction and active crustal earthquakes will be affected by different wave propagation paths, which is reflected in the variability in the path-component κ_R. Variations in $\Delta\kappa_0$ values at selected stations are relatively small for the

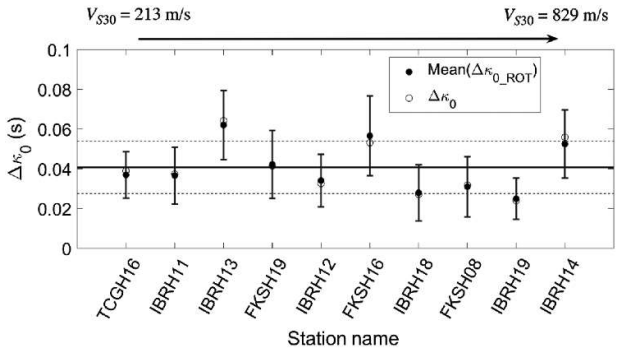

Figure 10. *Comparison of* $\text{mean}(\Delta\kappa(\theta))$ *and* $\Delta\kappa_0$ *at each station.* $\Delta\kappa_0$ *is the difference between surface and borehole* κ_0 *estimated from empirical regressions on as-recorded horizontal components. The error bar (within-station variability) represents* ± 1 *standard derivation of* $\Delta\kappa(\theta)$ *at each station. The horizontal solid line presents the mean of* $\Delta\kappa(\theta)$ *across all stations, and the dashed lines indicate the* ± 1 *standard derivation of* $\Delta\kappa(\theta)$ *across all considered stations (between-station variability).*

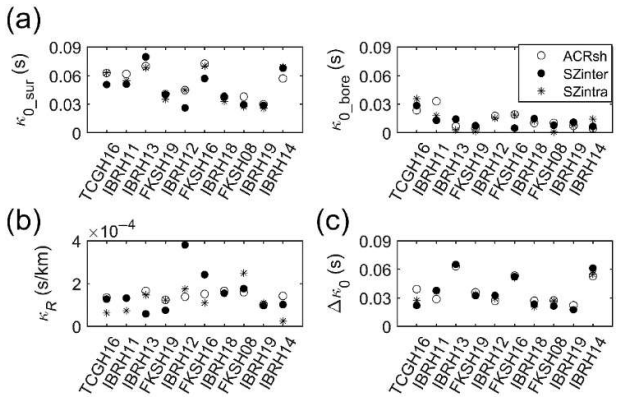

Figure 8. *Comparisons of (a)* κ_0 *(at the ground surface and at depth), (b)* κ_R*, and (c)* $\Delta\kappa_0$ *values for different earthquake types at each station. ACRsh, shallow active crustal; SZinter, subduction zone interface; SZintra, subduction zone intraslab.*

different datasets considered, which supports previous research indicating the site-specific nature of $\Delta\kappa_0$ values that is not affected by the

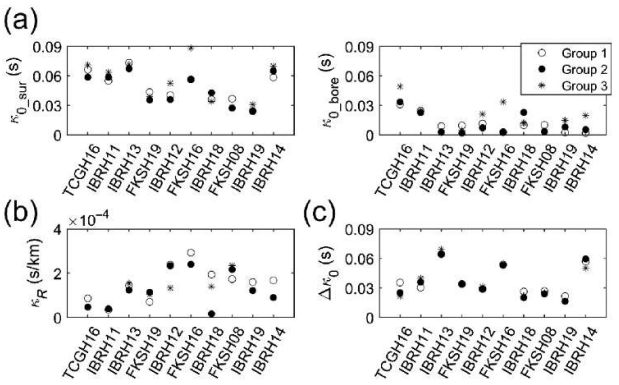

Figure 9. *Comparisons of (a)* κ_0 *(at the ground surface and at depth), (b)* κ_R*, and (c)* $\Delta\kappa_0$ *(the difference between surface and borehole* κ_0*) values for different focal depth groups at each station. Groups 1, 2, and 3 consider focal depths of less than 35 km, from 35 to 70 km, and more than 70 km, respectively.*

earthquake type (i.e., the difference between $\kappa_{0_{sur}}$ and $\kappa_{0_{bore}}$ represents the seismic attenuation taking place throughout the local soil column, Cabas et al., 2017).

The influence of focal depth on the estimations of κ_0 and κ_R is investigated by separating into three groups with focal depths of: (1) less than 35 km (which includes both ACRsh and SZintra events), (2) from 35 to 70 km (which includes the ACRde and SZintra events), and (3) more than 70 km (which includes the ACRde and SZinter events). A correlation between κ_R values and focal depth is not observed, but κ_R values show less variation when grouped by focal depth (regardless of earthquake type) than by earthquake type as seen in Figure 10.

The influence of earthquake type and focal depth is further explored in Figure 11, in which

TABLE 1
Selected Station Information

Station Name	Hole Depth (m)†	H_{800} (m)#	$V_{S,mean}$ (m/s)*	$\sigma(\Delta\kappa(\theta))$(s)†	Mean$(\Delta\kappa(\theta))$ (s)#	NEHRP Site Class§
IBRH14	100	10	1601,44	0,0172	0,0525	B
IBRH19	210	2	1792,68	0,0103	0,0249	C
FKSH08	105	8	936,59	0,0151	0,0310	C
IBRH18	504	30	1522,67	0,0142	0,0279	C
FKSH16	300	180	841,95	0,0201	0,0566	C
IBRH12	200	20	967,53	0,0132	0,0341	C
FKSH19	100	20	842,76	0,0170	0,0422	D
IBRH13	100	34	793,95	0,0174	0,0620	D
IBRH11	103	30	649,92	0,0143	0,0366	D
TCGH16	112	NaN	369,34	0,0138	0,0369	D

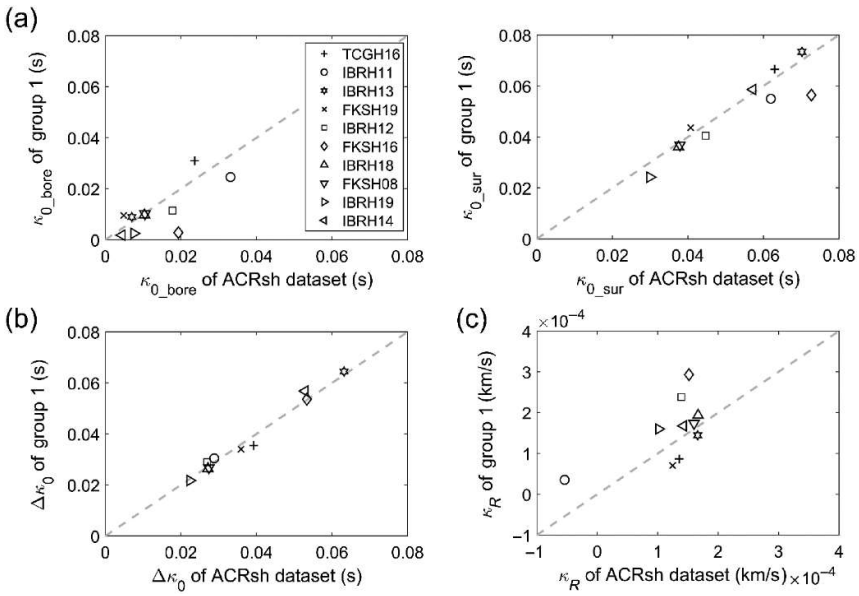

Figure 11. *Comparisons of (a) κ_0 (at the ground surface and at depth), (b) $\Delta\kappa_0$ (the difference between surface and borehole κ_0), and (c) κ_R values estimated with ACRsh dataset and group 1. Group 1 includes the events with focal depth less than 35 km (which includes both ACRsh and SZintra events).*

κ_R, κ_0, and $\Delta\kappa_0$ values estimated only using ACRsh events and a dataset of records with focal depth less than 35 km (i.e., group 1) are compared. It should be noted that a negative $\Delta\kappa_0$-value is derived at IBRH11 for the ACRsh datasets, which may be caused by the absence of events for epicentral distance less than 50 km. The average differences of $\Delta\kappa_0$ estimations between these two data sets across the 10 stations are 28.43% (neglecting the values at IBRH11), whereas the corresponding average differences of $\kappa_{0_{sur}}$ and $\Delta\kappa_0$ are 8.77% and 4.51%, respectively. The differences in κ_0, $\kappa_{0_{sur}}$, $\kappa_{0_{bore}}$, and $\Delta\kappa_0$ estimates are acceptable, which supports the incorporation of shallow subduction zone events to a shallow crustal event dataset. Estimates of κ_R and κ_0 for each group and earthquake types at the selected stations are shown in Table S1.

CONCLUSIONS

Repeatable contributions from path and site terms to the within-station variability in individual estimates of κ_r and site-specific κ_0 were investigated using 10 stations from the KiK-net database. Our dataset consisted of linear ground motions with surface PGA less than 0.01g, M_w larger than 4.0, and epicentral distance less than 150 km. Both active crustal and subduction earthquakes were used in this work to investigate repeatable contributions from the wave propagation path. Systematic variability on κr and κ_0 values stemming from the dataset choice, namely the selection of events based on their focal depth and type of seismicity, was evaluated. Contributions to the within-station variability associated with ground-motion directionality were also investigated.

The influence of ground-motion directionality on the estimates of $\kappa_{r_{AS}}$ was studied, and findings from this work revealed that the orientation of ground-motion affects estimates of $\kappa_{r_{AS}}$ computed on single horizontal components. However, this influence can be removed when calculating the average of two as-recorded horizontal component $\kappa_{r_{AS}}$ values. Thus, using the mean of two horizontal $\kappa_{r_{AS}}$ values (without considerations of the difference between these two values) is recommended as the representative κ-value for each ground-motion pair. This is different from previous recommendations to only report $\kappa_{r_{AS}}$ values for which differences between the recorded horizontal components are less than 20%. It was also found that the within-station variability in $\Delta\kappa_0$ values (i.e., the difference between κ_0 values at the surface and at depth) associated with directionality effects can be comparable to the between-station variability. This observation highlights the importance of quantifying the within-station variability on κ estimates in a more robust manner. Moreover, our findings support previous research efforts indicating that site

amplification effects on κ estimates should be minimized to obtain reliable estimates at sites of interest. Systematic contributions from event azimuths were not observed, whereas the variability in $\Delta\kappa(\theta)$ estimates with rotation angle was found to be a function of local soil conditions. The influence of ground-motion directionality on the parameterization of near-surface attenuation was found to be station dependent, but further investigation is required to identify relevant correlations between observed ground-motion directionality and site properties. Near-surface seismic attenuation anisotropy could help explain observed variations of $\Delta\kappa(\theta)$ with ground-motion orientation. Anisotropy in Q values has been observed from both laboratory experiments (Tao and King, 1990; Kern et al., 1997) and the analysis of earthquake ground motions (Liu et al., 2005). The random distributed cracks near surface could also cause seismic anisotropy (Liu et al., 1993; Boness and Zoback, 2004; Liu et al., 2004), which could then influence seismic-wave scattering and reflection. The specific geological condition and volcanic environment in Japan also lead to anisotropy in Q (Pei et al., 2009; Nakano et al., 2015). More generally, a preferred direction of ground-motion independent from the expected polarization (based on focal mechanism and location of the events) has also been observed in recorded data from the Whittier Narrows and Loma Prieta earthquakes (Bonamassa et al., 1991; Bonamassa and Vidale, 1991). More research on directionality effects is required to elucidate the physical basis for the observed variation of attenuation characteristics of ground motions with orientation. Different earthquake types were found to lead to different κ_R values. However, it is important that the classification of seismicity type is also tied to the focal depth. Selecting a dataset with considerations of systematic variations stemming from varying focal depths and earthquake types is recommended to resolved κ's path component, κ_R more reliably. Deep earthquakes can produce multiwave propagation paths to the site of interest, which could have a more significant influence on κ_R. On the other hand, the incidence angle of seismic waves when the focal depth is shallow could introduce larger within-station variability. Smaller differences in surface and borehole κ_0 values were observed across the datasets used (i.e., different focal depths or earthquake types). The lack of variability of $\Delta\kappa_0$ values as a function of source and path effects evidences that $\Delta\kappa_0$ is mainly a function of near-surface attenuation, which supports its site-specific nature also observed in previous research studies.

DATA AND RESOURCES

Accelerograms and geotechnical data are obtained from the KiK-net network at http://www.kyoshin.bosai.go.jp (last accessed December 2018), collected and distributed by National Research Institute for Earth Science and Disaster Prevention (NIED). The orientations of borehole sensors are available at http://www.hinet.bosai.go.jp/st_info/detail/?LANG=ja (last accessed December 2018). The earthquake information is available F-net network at http://www.fnet.bosai.go.jp/top.php (last accessed December 2018). The supplemental material to this article includes one table, which contains κ values of different datasets classified by earthquake type and focal depth, and two figures, which provide the additional comparisons to show the influence of ground-motion directionality on κ estimations.

ACKNOWLEDGMENTS

The authors appreciate that the National Research Institute for Earth Science and Disaster Prevention (NIED) provides the data for this work. The authors acknowledge Haitham Dawood and Adrian Rodriguez-Marek for providing their processed dataset. The authors are thankful to Associate Editor Martin Chapman, Benjamin Edwards, and one anonymous reviewer for the useful comments. This study was sponsored by the Internationalization Seed Grant at NC State University and the U.S. Geological Survey (USGS) under Grant Number G18AS00021. The views and conclusions contained in this document are those of the authors and should not be interpreted as representing the opinions or policies of the USGS.

REFERENCES

Al Atik, L., N. A. Abrahamson, J. J. Bommer, F. Scherbaum, F. Cotton, and N. Kuehn (2010). The variability of ground-motion prediction models

and its components, Seismol. Res. Lett. 81, no. 5, 794–801.

Al Atik, L., A. Kottke, N. Abrahamson, and J. Hollenback (2014). Kappa (κ) scaling of ground-motion prediction equations using an inverse random vibration theory approach, Bull. Seismol. Soc. Am. 104, no. 1, 336–346.

Anderson, J. G. (1991). A preliminary descriptive model for the distance dependence of the spectral decay parameter in southern California, Bull. Seismol. Soc. Am. 81, no. 6, 2186–2193.

Anderson, J. G., and S. E. Hough (1984). A model for the shape of the Fourier amplitude spectrum of acceleration at high frequencies, Bull. Seismol. Soc. Am. 74, no. 5, 1969–1993.

Aoi, S., T. Kunugi, and H. Fujiwara (2004). Strong-motion seismograph network operated by NIED: K-NET and KiK-net, J. Japan Assoc. Earthq. Eng. 4, no. 3, 65–74.

Aoi, S., T. Kunugi, H. Nakamura, and H. Fujiwara (2011). Deployment of new strongmotion seismographs of K-NET and KiK-net, Geotech. Geol. Earthq. Eng. 14, 167–186, doi: 10.1007/978-94-007-0152-6_12.

Baltay, A. S., T. C. Hanks, and N. A. Abrahamson (2017). Uncertainty, variability, and earthquake physics in ground-motion prediction equations, Bull. Seismol. Soc. Am. 107, no. 4, 1754–1772.

Biasi, G. P., and K. D. Smith (2001). Site Effects for Seismic Monitoring Stations in the Vicinity of Yucca Mountain, Nevada, MOL20011204.0045, A Report prepared for the US DOE/University and Community College System of Nevada (UCCSN) Cooperative Agreement.

Bommer, J. J., and N. A. Abrahamson (2006). Why do modern probabilistic seismic-hazard analyses often lead to increased hazard estimates? Bull. Seismol. Soc. Am. 96, no. 6, 1967–1977.

Bonamassa, O., and J. E. Vidale (1991). Directional site resonances observed from aftershocks of the 18 October 1989 Loma Prieta earthquake, Bull. Seismol. Soc. Am. 81, no. 5, 1945–1957.

Bonamassa, O., J. E. Vidale, H. Houston, and S. Y. Schwartz (1991). Directional site resonances and the influence of near-surface geology on ground motion, Geophys. Res. Lett. 18, no. 5, 901–904.

Boness, N., and M. D. Zoback (2004). Stress-induced seismic velocity anisotropy and physical properties in the SAFOD pilot hole in Parkfield, CA, Geophys. Res. Lett. 31, L15S17, doi: 10.1029/2003GL019020.

Boore, D. M. (2010). Orientation-independent, nongeometric-mean measures of seismic intensity from two horizontal components of motion, Bull. Seismol. Soc. Am. 100, no. 4, 1830–1835.

Boore, D. M., J. Watson-Lamprey, and N. A. Abrahamson (2006). Orientation-independent measures of ground motion, Bull. Seismol. Soc. Am. 96, no. 4A, 1502–1511.

Brune, J. N. (1970). Tectonic stress and the spectra of seismic shear waves from earthquakes, J. Geophys. Res. 75, no. 26, 4997–5009.

Brune, J. N. (1971). Correction to "Tectonic stress and the spectra of seismic shear waves from earthquakes" J. Geophys. Res. 76, 5002.

Cabas, A., and A. Rodriguez-Marek (2017). VS-κ 0 correction factors for input ground motions used in seismic site response analyses, Earthq. Spectra 33, no. 3, 917–941.

Cabas, A., A. Rodriguez-Marek, and L. F. Bonilla (2017). Estimation of site-specific kappa (κ0)-consistent damping values at KiK-net sites to assess the discrepancy between laboratory-based damping models and observed attenuation (of seismic waves) in the field, Bull. Seismol. Soc. Am. 107, no. 5, 2258–2271.

Campbell, K. W. (2003). Prediction of strong ground motion using the hybrid empirical method and its use in the development of ground-motion (attenuation) relations in eastern North America, Bull. Seismol. Soc. Am. 93, no. 3, 1012–1033.

Campbell, K. W. (2009). Estimates of shear-wave Q and κ_0 for unconsolidated and semiconsolidated sediments in Eastern North America, Bull. Seismol. Soc. Am. 99, no. 4, 2365–2392.

Dawood, H. M., A. Rodriguez-Marek, J. Bayless, C. Goulet, and E. Thompson (2016). A flatfile for the KiK-net database processed using an automated protocol, Earthq. Spectra 32, no. 2, 1281–1302.

Dimitriu, P., N. Theodulidis, P. Hatzidimitriou, and A. Anastasiadis (2001). Sediment non-linearity and attenuation of seismic waves: A study of accelerograms from Lefkas, western Greece, Soil Dynam. Earthq. Eng. 21, no. 1, 63–73.

Douglas, J., P. Gehl, L. F. Bonilla, and C. Gélis (2010). A κ model for mainland France, Pure Appl. Geophys. 167, no. 11, 1303–1315.

Drouet, S., F. Cotton, and P. Guéguen (2010). v S 30, κ, regional attenuation and Mw from accelerograms: Application to magnitude 3–5 French earthquakes, Geophys. J. Int. 182, no. 2, 880–898.

Edwards, B., O. J. Ktenidou, F. Cotton, N. Abrahamson, C. Van Houtte, and D. Fäh (2015). Epistemic uncertainty and limitations of the κ_0 model for near-surface attenuation at hard rock sites, Geophys. J. Int. 202, no. 3, 1627–1645.

Fujiwara, H., S. Aoi, T. Kunugi, and S. Adachi (2004). Strong-Motion Observation Networks of NIED: K-NET and KiK-net, Technical report, Consortium of Organizations for Strong-Motion Observation Systems (COSMOS), https://www.yumpu.com/en/document/read/18306131/strong-motion-observation-networks-of-nied-k-net-and-cosmos (last accessed February 2020).

Garcia, D., D. J. Wald, and M. G. Hearne (2012). A global earthquake discrimination scheme to optimize ground-motion prediction equation selection, Bull. Seismol. Soc. Am. 102, no. 1, 185–203.

Kern, H., B. Liu, and T. Popp (1997). Relationship between anisotropy of P and S wave velocities and anisotropy of attenuation in serpentinite and amphibolite, J. Geophys. Res. 102, no. B2, 3051–3065.

Knopoff, L. (1964). Q, Rev. Geophys. 2, no. 4, 625–660.

Kotha, S. R., F. Cotton, and D. Bindi (2019). Empirical models of shear-wave radiation pattern derived from large datasets of ground-shaking observations, Sci. Rep. 9, no. 1, 1–11.

Ktenidou, O. J., N. Abrahamson, R. Darragh, and W. Silva (2016). A methodology for the estimation of kappa (κ) from large datasets, example application to rock sites in the NGA-East database, and implications on design motions, PEER Rept. 2016, Vol. 1, https://peer.berkeley.edu/sites/default/files/2016-01_olga-joan_ktenidou_norman_a._abrahamson_robert_b._darragh_walter_j._silva.pdf (last accessed September 2017).

Ktenidou, O. J., N. A. Abrahamson, S. Drouet, and F. Cotton (2015). Understanding the physics of kappa (κ): Insights from a downhole array, Geophys. J. Int. 203, no. 1, 678–691.

Ktenidou, O. J., F. Cotton, N. A. Abrahamson, and J. G. Anderson (2014). Taxonomy of κ: A review of definitions and estimation approaches targeted to applications, Seismol. Res. Lett. 85, no. 1, 135–146.

Ktenidou, O. J., C. Gélis, and L. F. Bonilla (2013). A study on the variability of kappa (κ) in a borehole: Implications of the computation process, Bull. Seismol. Soc. Am. 103, no. 2A, 1048–1068.

Kuehn, N. M., N. A. Abrahamson, and M. A. Walling (2019). Incorporating nonergodic path effects into the NGA-West2 ground-motion prediction equations, Bull. Seismol. Soc. Am. 109, no. 2, 575–585.

Laurendeau, A., F. Cotton, O. J. Ktenidou, L. F. Bonilla, and F. Hollender (2013). Rock and stiff-soil site amplification: Dependency on VS30 and kappa (κ 0), Bull. Seismol. Soc. Am. 103, no. 6, 3131–3148.

Liu, E., S. Crampin, J. H. Queen, and W. D. Rizer (1993). Velocity and attenuation anisotropy caused by microcracks and macrofractures in a multiazimuth reverse VSP, Can. J. Explor. Geophys. 29, no. 1, 177–188.

Liu, Y., T. L. Teng, and Y. Ben-Zion (2004). Systematic analysis of shear-wave splitting in the aftershock zone of the 1999 Chi-Chi, Taiwan, earthquake: Shallow crustal anisotropy and lack of precursory variations, Bull. Seismol. Soc. Am. 94, no. 6, 2330–2347.

Liu, Y., T. L. Teng, and Y. Ben-Zion (2005). Near-surface seismic anisotropy, attenuation and dispersion in the aftershock region of the 1999 Chi-Chi earthquake, Geophys. J. Int. 160, no. 2, 695–706.

Mayor, J., S. S. Bora, and F. Cotton (2018). Capturing regional variations of hard-rock κ 0 from coda analysis, Bull. Seismol. Soc. Am. 108, no. 1, 399–408.

Nakano, K., S. Matsushima, and H. Kawase (2015). Statistical properties of strong ground motions from the generalized spectral inversion of data observed by K-NET, KiK-net, and the JMA Shindokei network in Japan, Bull. Seismol. Soc. Am. 105, no. 5, 2662–2680.

Oth, A., S. Parolai, and D. Bindi (2011). Spectral analysis of K-NET and

KiK-net data in Japan, Part I: Database compilation and peculiarities, Bull. Seismol. Soc. Am. 101, no. 2, 652–666.

Parolai, S. (2018). κ0: Origin and usability, Bull. Seismol. Soc. Am. 108, no. 6, 3446–3456.

Parolai, S., and D. Bindi (2004). Influence of soil-layer properties on k evaluation, Bull. Seismol. Soc. Am. 94, no. 1, 349–356.

Parolai, S., D. Bindi, and M. Pilz (2015). k0: The role of intrinsic and scattering attenuation, Bull. Seismol. Soc. Am. 105, no. 2A, 1049–1052.

Pei, S., Z. Cui, Y. Sun, M. N. Toksöz, C. A. Rowe, X. Gao, and F. D. Morgan (2009). Structure of the upper crust in Japan from S-wave attenuation tomography, Bull. Seismol. Soc. Am. 99, no. 1, 428–434.

Perron, V., F. Hollender, P. Y. Bard, C. Gélis, C. Guyonnet-Benaize, B. Hernandez, and O. J. Ktenidou (2017). Robustness of kappa (κ) measurement in low-to-moderate seismicity areas: Insight from a site-specific study in Provence, France, Bull. Seismol. Soc. Am. 107, no. 5, 2272–2292.

Pilz, M., and F. Cotton (2019). Does the 1D assumption hold for site response analysis? A study of seismic site responses and implication for ground motion assessment using KiK-net strong-motion data, Earthq. Spectra 35, no. 2, 883–905.

Pilz, M., and D. Fäh (2017). The contribution of scattering to nearsurface attenuation, J. Seismol. 21, no. 4, 837–855.

Pilz, M., F. Cotton, R. Zaccarelli, and D. Bindi (2019). Capturing regional variations of hard-rock attenuation in Europe, Bull. Seismol. Soc. Am. 109, no. 4, 1401–1418.

Rodriguez-Marek, A., E. M. Rathje, J. J. Bommer, F. Scherbaum, and P. J. Stafford (2014). Application of single-station sigma and site-response characterization in a probabilistic seismic-hazard analysis for a new nuclear site, Bull. Seismol. Soc. Am. 104, no. 4, 1601–1619.

Silva, W. J., and R. Darragh (1995). Engineering Characterization of Earthquake Strong Ground Motion Recorded at Rock Sites, Electric Power Research Institute, Palo Alto, California, TR–102261.

Tao, G., and M. S. King (1990). Shear-wave velocity and Q anisotropy in rocks: A laboratory study, Int. J. Rock Mech. Min. Sci. Geomech. Abstr. 27, 353–361.

Van Houtte, C., S. Drouet, and F. Cotton (2011). Analysis of the origins of κ (kappa) to compute hard rock to rock adjustment factors for GMPEs, Bull. Seismol. Soc. Am. 101, no. 6, 2926–2941.

Van Houtte, C., O. J. Ktenidou, T. Larkin, and C. Holden (2014). Hard-site κ_0 (kappa) calculations for Christchurch, New Zealand, and comparison with local ground-motion prediction models, Bull. Seismol. Soc. Am. 104, no. 4, 1899–1913.

Wu, H., K. Masaki, K. Irikura, and F. J. Sánchez-Sesma (2017). Application of a simplified calculation for full-wave microtremor H/V spectral ratio based on the diffuse field approximation to identify underground velocity structures, Earth Planets Space 69, no. 1, 162.

Xu, B., E. M. Rathje, Y. Hashash, J. Stewart, K. Campbell, and W. J. Silva (2019). κ0 for soil sites: Observations from Kik-net sites and their use in constraining small-strain damping profiles for site response analysis, Earthq. Spectra 36, no. 1, 111–137.